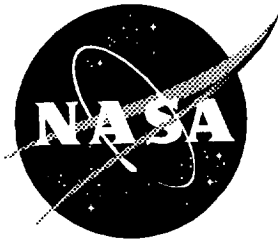NASA/TM-2000-210628

Use of Guided Acoustic Waves to Assess the Effects of Thermal-Mechanical Cycling on Composite Stiffness

Michael D. Seale and Eric I. Madaras
Langley Research Center, Hampton, Virginia

December 2000

The NASA STI Program Office . . . in Profile

Since its founding, NASA has been dedicated to the advancement of aeronautics and space science. The NASA Scientific and Technical Information (STI) Program Office plays a key part in helping NASA maintain this important role.

The NASA STI Program Office is operated by Langley Research Center, the lead center for NASA's scientific and technical information. The NASA STI Program Office provides access to the NASA STI Database, the largest collection of aeronautical and space science STI in the world. The Program Office is also NASA's institutional mechanism for disseminating the results of its research and development activities. These results are published by NASA in the NASA STI Report Series, which includes the following report types:

- TECHNICAL PUBLICATION. Reports of completed research or a major significant phase of research that present the results of NASA programs and include extensive data or theoretical analysis. Includes compilations of significant scientific and technical data and information deemed to be of continuing reference value. NASA counterpart or peer-reviewed formal professional papers, but having less stringent limitations on manuscript length and extent of graphic presentations.

- TECHNICAL MEMORANDUM. Scientific and technical findings that are preliminary or of specialized interest, e.g., quick release reports, working papers, and bibliographies that contain minimal annotation. Does not contain extensive analysis.

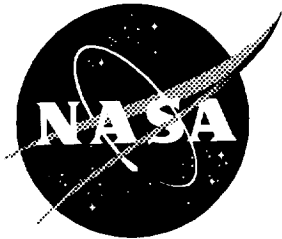- CONTRACTOR REPORT. Scientific and technical findings by NASA-sponsored contractors and grantees.

- CONFERENCE PUBLICATION. Collected papers from scientific and technical conferences, symposia, seminars, or other meetings sponsored or co-sponsored by NASA.

- SPECIAL PUBLICATION. Scientific, technical, or historical information from NASA programs, projects, and missions, often concerned with subjects having substantial public interest.

- TECHNICAL TRANSLATION. English-language translations of foreign scientific and technical material pertinent to NASA's mission.

Specialized services that complement the STI Program Office's diverse offerings include creating custom thesauri, building customized databases, organizing and publishing research results . . . even providing videos.

For more information about the NASA STI Program Office, see the following:

- Access the NASA STI Program Home Page at *http://www.sti.nasa.gov*

- Email your question via the Internet to help@sti.nasa.gov

- Fax your question to the NASA STI Help Desk at (301) 621-0134

- Telephone the NASA STI Help Desk at (301) 621-0390

- Write to:
  NASA STI Help Desk
  NASA Center for AeroSpace Information
  7121 Standard Drive
  Hanover, MD 21076-1320

NASA/TM-2000-210628

Use of Guided Acoustic Waves to Assess the Effects of Thermal-Mechanical Cycling on Composite Stiffness

Michael D. Seale and Eric I. Madaras
Langley Research Center, Hampton, Virginia

December 2000

Acknowledgments

Available from:

NASA Center for AeroSpace Information (CASI)
7121 Standard Drive
Hanover, MD 21076-1320
(301) 621-0390

National Technical Information Service (NTIS)
5285 Port Royal Road
Springfield, VA 22161-2171
(703) 605-6000

Abstract

The introduction of new, advanced composite materials into aviation systems requires a thorough understanding of the long-term effects of combined thermal and mechanical loading. As part of a study to evaluate the effects of thermal-mechanical cycling, a guided acoustic (Lamb) wave measurement system was used to measure the bending and out-of-plane stiffness coefficients of composite laminates undergoing thermal-mechanical loading. The system uses a pulse/ receive technique that excites an antisymmetric Lamb mode and measures the time-of-flight over a wide frequency range. Given the material density and plate thickness, the bending and out-of-plane shear stiffnesses are calculated from a reconstruction of the velocity dispersion curve. A series of 16 and 32-ply composite laminates were subjected to a thermal-mechanical loading profile in load frames equipped with special environmental chambers. The composite systems studied were a graphite fiber reinforced amorphous thermoplastic polyimide and a graphite fiber reinforced bismaleimide thermoset. The samples were exposed to both high and low temperature extremes as well as high and low strain profiles. The bending and out-of-plane stiffnesses for composite samples that have undergone over 6,000 cycles of thermal-mechanical loading are reported. The Lamb wave generated elastic stiffness results have shown decreases of up to 20% at 4,936 loading cycles for the graphite/thermoplastic samples and up to 64% at 4,706 loading cycles for the graphite/thermoset samples.

Introduction

Advanced composite materials, which are gaining wide use in a variety of structural applications, are required to operate under severe environmental conditions for thousands of hours. In such environments, deterioration with age can cause a significant decrease in the load-carrying capability of these materials, which could compromise safety. Therefore, techniques are required to nondestructively evaluate the integrity of composites which will be subjected to these hostile operating conditions.

Among the various techniques available, guided acoustic waves (Lamb waves) offer a convenient method of evaluating these composite materials. As shown by Karim, et al.[1] and Mal, et al.,[2] inversion techniques can be used to ascertain the material parameters of composites from experimental Lamb wave data.

Studies have been conducted which show a reduction in Lamb wave velocity due to a loss of stiffness caused by matrix cracking.[3-7] Seale, et al.[3] showed a correlation between Lamb wave velocity and stiffness measured with strain gages as well as a correlation between Lamb wave velocity and crack density for mechanically fatigued composite samples. Dayal and Kinra[4] showed that for Lamb wave propagation in the plane of the plate, both wavespeed and attenuation were sensitive to cracking. Tang and Henneke[5] noted that Lamb waves provide information about the in-plane elastic properties of a plate. This type of measurement is more useful due to the fact that composites are commonly designed to carry in-plane loads. Similarly, Dayal, et al.[6] noted that the Lamb wave interaction with cracks is much stronger in the plane of the plate and, thus, provides an effective method to detect damage due to transverse matrix cracking. Recently, Shih, et al.[7] used measurements of the extensional Lamb mode velocity to calculate laminate stiffness constants in mechanically fatigued composites.

Under general thermal-mechanical loading, thermal degradation as well as mechanical fatigue damage may occur. The above studies[3-7] illustrate the use of Lamb waves to examine mechanical fatigue damage. However, in only a few cases[3,8] have ultrasonic non-destructive evaluation techniques been used for assessing either thermal degradation or thermal-mechanical cycling in polymer matrix composites. Ultrasonic Lamb waves have been shown by Seale, et al.[3] and Bar-Cohen, et al.[8] to be an effective method for characterizing thermal damage in composites.

In this study, a scanning system was used to measure the Lamb wave velocity over a wide frequency range for composites which were subjected to thermal-mechanical cycling. From the Lamb wave velocity data, the bending and out-of-plane stiffness values were determined for each of the specimens. The following section will describe the composites studied as well as the loading profile to which these samples were subjected. This will be followed by a brief summary of laminated plate theory and the process of reconstructing the velocity dispersion curve to obtain material stiffness values. A description of the Lamb wave scanning system and an evaluation of the accuracy of the measurement technique is then presented. The ensuing section describes the stiffness measurements on the composite samples. Finally, the results for samples which have been undergone up to 6,000 loading cycles are presented and the effectiveness of the Lamb wave technique in measuring thermal-mechanical damage in composites is discussed.

Composite Materials and Thermal-Mechanical Loading Profile

The composite materials studied were a graphite fiber reinforced amorphous thermoplastic polyimide, IM7/K3B, and a graphite fiber reinforced bismaleimide thermoset, IM7/5260. The samples were manufactured with 16 and 32 plies and had stacking sequences of $[45/0/-45/90]_{2S}$ and $[45/0/-45/90]_{4S}$, respectively. The size of all of the samples was 122-cm by 30.5-cm. The IM7/K3B samples were all constructed with 16 plys and had a nominal thickness of 0.223 cm. The IM7/5260 specimens consisted of both 16 and 32-ply architectures and had nominal thicknesses of 0.248 cm and 0.483 cm, respectively.

Thermal-mechanical cycling of the samples was performed in either 98-kN (22-kip) or 222-kN (50-kip) capacity load frames equipped with environmental chambers which had a usable temperature range of -54 °C to +344 °C. The chamber dimensions were 40-cm wide by 67-cm tall by 40-cm deep. Thus, the upper and lower portions of the samples remained outside of the chambers and only the middle 67-cm section along the length of each of the samples was subjected to thermal extremes. A photo of an environmental chamber is shown in Fig. 1 and an image of a composite sample is shown in Fig. 2.
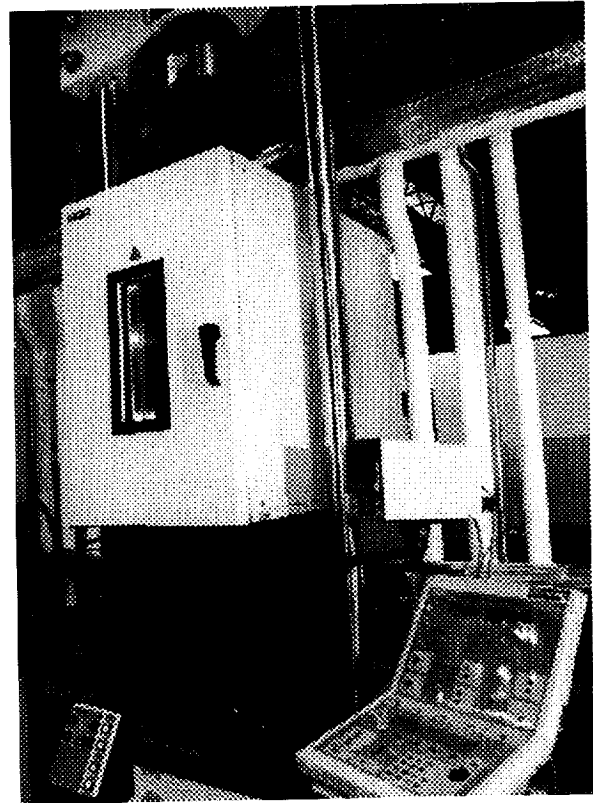

Figure 1. Photo of an environmental chamber and load frame used to subject the composite samples to thermal-mechanical loading.
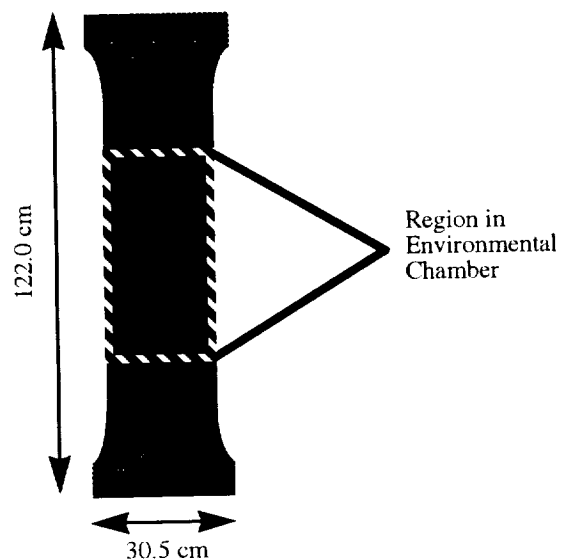

Figure 2. Image of a sample showing the region in the environmental chamber.

2

For all of the samples, the load was applied in the 0° direction (along the length of the specimens). Both high and low strain profiles as well as high and low temperature profiles were used. The low-strain profiles had strain levels which ranged from 0 to 2,000 microstrain with a sustained strain at or above 1,040 microstrain for 180 minutes. The high-strain profiles had strain levels which ranged from 0 to 3,000 microstrain with a sustained strain at or above 1,560 microstrain for 180 minutes. The temperature extremes for the high-temperature cycling were chosen to be -18 °C and +177 °C with a sustained temperature of +177 °C for 180 minutes. The temperature extremes for the low-temperature cycling were chosen to be -18 °C and +135 °C with a sustained temperature of +135 °C for 180 minutes. Each loading cycle lasted for a total of 255 minutes.

The thermal-mechanical loading profile used for this study is shown in Fig. 3. In the figure, the temperature and strain axes have been normalized to the values of temperature and strain which were maintained for a duration of 180 minutes for each cycle. The IM7/K3B samples were subjected to high temperature profiles and both high and low strain profiles. The 16-ply IM7/5260 samples were subjected to low strain levels and high and low temperature profiles. The 32-ply IM7/5260 samples were exposed to low temperature and high strain profiles only. The various profiles for the samples are summarized in Table I.
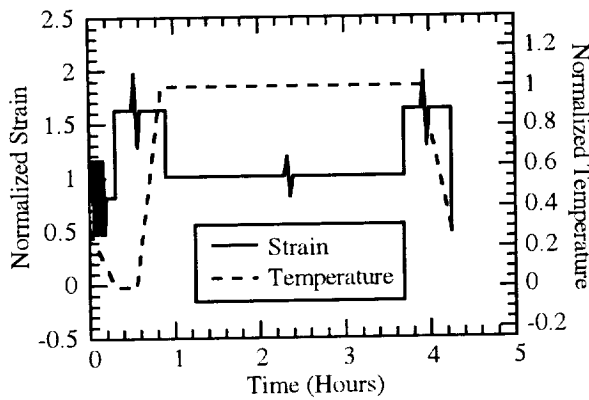
Table I. Test Matrix for Composite Samples.

Loading Profile	IM7/K3B	IM7/5260
Low Strain/ Low Temp.		16 Ply
Low Strain/ High Temp.	16 Ply	16 Ply
High Strain/ Low Temp.		32 Ply
High Strain/ High Temp.	16 Ply	

Laminated Plate Theory

Consider a composite lamina with the 1-axis defined as along the fiber direction, the 2-axis transverse to the fibers, and the 3-axis being out of the plane of the plate. For a lamina assumed to be under plane stress, the stress-strain relationship is given by[9]

$$\begin{bmatrix} Q_{11} & Q_{12} & 0 & 0 & 0 \\ Q_{12} & Q_{22} & 0 & 0 & 0 \\ 0 & 0 & Q_{44} & 0 & 0 \\ 0 & 0 & 0 & Q_{55} & 0 \\ 0 & 0 & 0 & 0 & Q_{66} \end{bmatrix} \begin{bmatrix} \varepsilon_1 \\ \varepsilon_2 \\ \gamma_{23} \\ \gamma_{31} \\ \gamma_{12} \end{bmatrix} \tag{1}$$

where σ and τ represent the stresses and ε and γ represent the strains. The Q_{ij} are the plane-stress stiffness components for $i, j = 1, 2, 6$ and the shear stiffness components for $i, j = 4, 5$.

Composite laminates often consist of individual lamina with the fibers oriented at various angles with respect to the structural axes (see Fig. 4). The angle θ is defined as positive for a counterclockwise rotation from the laminate (x-y) axes to the individual lamina (1-2) axes. The bending stiffnesses, D_{ij}, and the out-of-plane stiffnesses, A_{jj}, for the entire laminate are obtained by integrating the Q_{ij} through the thickness of the plate. These stiffness values are defined as[10]

Figure 3. Thermal-mechanical loading profile.

$$D_{ij} = \int_{-\frac{h}{2}}^{\frac{h}{2}} (Q_{ij}')_k z^2 dz \qquad i, j = 1, 2, 6 \tag{2}$$
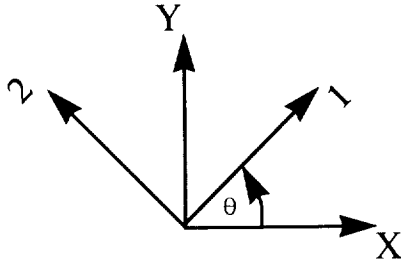
3

Figure 4. Rotation of coordinate system from the lamina (1-2) axes to the laminate (x-y) axes.

and

$$A_{jj} = k_j^2 \int_{-\frac{h}{2}}^{\frac{h}{2}} (Q_{jj}')_k dz \qquad j = 4, 5 \qquad (3)$$

where h is the total thickness of the plate, the subscript k represents each layer in the laminate, and k_j is a shear correction factor. The Q_{ij}' represent the transformed stiffness coefficients rotated according to the orientation of each ply with respect to the structural axes.

Lamb Waves and Plate Theory Approximations

Lamb waves arise from a coupling between the shear-vertical (SV) and compressional (P) waves reflected at the stress-free boundaries at the top and bottom of a thin plate. The Lamb mode solutions are grouped into two classes which are defined in terms of the symmetry of the displacements of the plate with respect to the mid-plane. The modes are labeled as symmetric, S_n, and antisymmetric, A_n. For reference, the Lamb wave dispersion curves for the first three symmetric and antisymmetric modes in the composite samples used in this study are shown in Fig. 5. The dispersion curves shown in the figure were generated using a through-the-thickness finite element model, detailed in Dong and Huang[11] and Datta, et al.[12] As can be seen from the figure, higher order symmetric and antisymmetric modes begin to propagate as the frequency increases. However, at frequencies below 500 kHz, only the lowest order symmetric mode, S_0, and lowest order antisymmetric mode, A_0, propagate.

In this region, the S_0, or extensional plate mode, is almost nondispersive and the A_0, or flexural plate mode, is highly dispersive. Since this study uses velocity measurements for the flexural mode, only those solutions will be treated here.
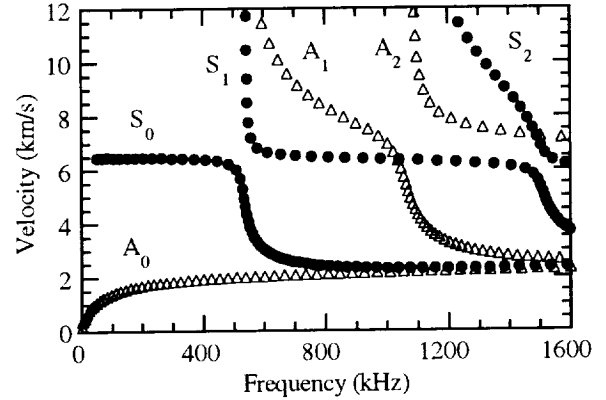

Figure 5. Lamb wave dispersion curves showing the symmetric (solid circles) and antisymmetric (open triangles) modes.

Flexural mode equations

For a symmetric quasi-isotropic plate, the dispersion relation for the flexural plate mode propagating in the 0° direction (along the structural x-axis) is given by[10]

$$[(D_{11}k^2 + A_{55} - I\omega^2)(D_{66}k^2 + A_{44} - I\omega^2)$$
$$(A_{55}k^2 - \rho^*\omega^2)] - (D_{16}k^2)^2(A_{55}k^2 - \rho^*\omega^2) \qquad (4)$$
$$- (A_{55}k)^2(D_{66}k^2 + A_{44} - I\omega^2) = 0$$

For waves propagating in the 90° direction of a symmetric quasi-isotropic plate, the relation is[10]

$$[(D_{22}k^2 + A_{44} - I\omega^2)(D_{66}k^2 + A_{55} - I\omega^2)$$
$$(A_{44}k^2 - \rho^*\omega^2)] - (D_{16}k^2)^2(A_{44}k^2 - \rho^*\omega^2) \qquad (5)$$
$$- (A_{44}k)^2(D_{66}k^2 + A_{55} - I\omega^2) = 0$$

In the equations, ω is the angular frequency and k is the wavenumber. I and ρ^* are defined as[13]

4

$$I = \int\limits_{-\frac{h}{2}}^{\frac{h}{2}} \rho \, dz \qquad (6)$$

and

$$\rho^* = \int\limits_{-\frac{h}{2}}^{\frac{h}{2}} \rho z^2 dz \qquad (7)$$

where ρ is the density and h is the plate thickness. Multiple roots exist for the dispersion relations given by Eqs. (4) and (5). However, as evidenced by Fig. 5, only those which satisfy the condition that the velocity approaches zero as the frequency approaches zero are the ones corresponding to the A_0 mode. If the density, thickness, and stiffnesses are known, the dispersion curve can be obtained by selecting wavenumbers, k, and solving Eqs. (4) and (5) for the corresponding angular frequencies, ω. Once ω and k are known, the phase velocity, v, is given by

$$v = \frac{\omega}{k} \qquad (8)$$

and the frequency, f, is obtained from the angular frequency by using the relation

$$f = \frac{\omega}{2\pi} \cdot \qquad (9)$$

The dispersion curve is then generated by plotting the velocity as a function of frequency. For a further description of plate theory and how the laminate stiffnesses relate to the flexural wave velocity, the reader is referred to Tang, et al.[10]

Effects of Stiffness on Velocity

For propagation in the 0° direction, the effects of altering A_{55} and D_{11} on the flexural dispersion relation given by Eq. (4) are shown in Fig. 6. Decreasing the values of D_{16}, D_{66}, and A_{44} by 25% did not significantly alter the dispersion curve for Lamb wave propagation in the 0° direction and were omitted from the

figure for clarity. The effects of altering these three parameters are shown in Fig. 7. In Fig. 6, it can be seen that decreasing A_{55} by 25% alters the curve by a significant amount while a smaller shift in the curve is seen when D_{11} is reduced by 25%.
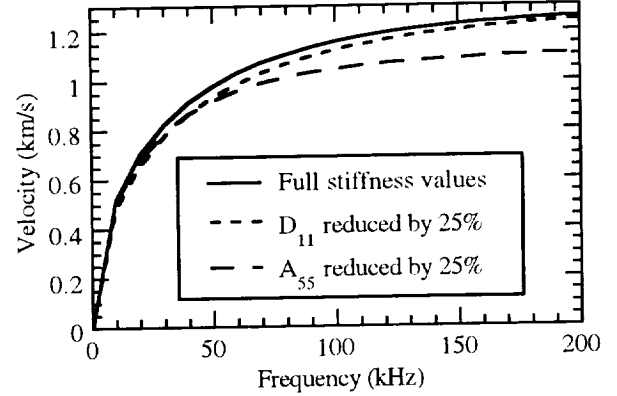

Figure 6. Flexural dispersion curves using full values of D_{11}, D_{16}, D_{66}, A_{44}, and A_{55}, with D_{11} reduced by 25%, and with A_{55} reduced by 25%. The curves with reduced values of D_{16}, D_{66}, and A_{44} are not be discernible from the curve constructed using the full stiffness values.

Shown in Fig. 7 is a plot of the percent change in velocity as a function of frequency for 25% reductions in each stiffness value. The figure clearly shows that the only constants which change the velocity by more than 0.5% are D_{11} and A_{55}. Also, changing D_{11} has a greater effect on the velocity at lower frequencies while changes in A_{55} alter the dispersion curve at higher frequencies. The dispersion curve for propagation in the 90° direction (along the structural y-axis) given by Eq. (5) has the same trends as seen in Fig. 6, except the constants controlling the behavior are D_{22} and A_{44}. The values of D_{16}, D_{66}, and A_{55} do not significantly affect the dispersion curve for Lamb waves propagating in the 90° direction. As with propagation in the 0° direction, these values will be held constant and the values of D_{22} and A_{44} will be used to fit the experimental data.

Lamb Wave Scanning System

The system used in this study, Lamb Wave Imager[TM] (LWI), is a commercial ultrasonic scanner developed by Digital Wave Corporation (DWC) in
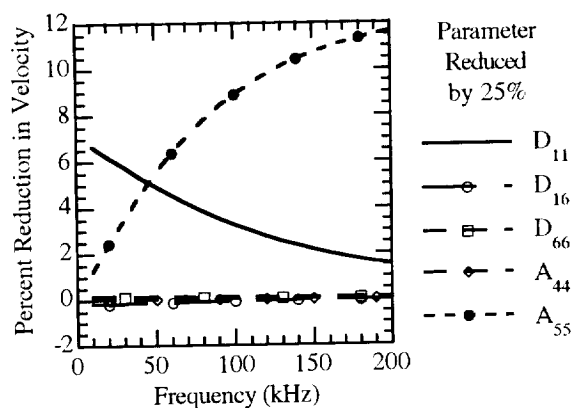
5

Figure 7. Plot of the percent reduction in velocity as a function of frequency for a 25% decrease in each stiffness constant.

Englewood, Colorado. It is capable of measuring the elastic properties for isotropic as well as anisotropic materials. The system consists of a scanner, scanner control unit, a pair of transducers, and a computer. The scanning control and data analysis is performed by a commercial software package developed by DWC. A schematic of the system is shown in Fig. 8.
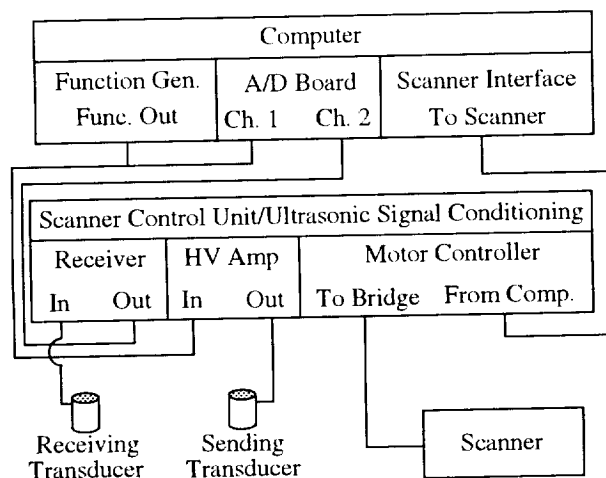

Figure 8. Schematic of the Lamb Wave Imager.[TM]

The scanner control unit incorporates a receiver, a high-voltage amplifier, and a motor controller. The receiver has an amplification range from 0 to 66 dB. The high-voltage amplifier is used to amplify the pulse used to drive the sending transducer. It has a bandwidth of 12 kHz to 1 MHz and a maximum output of

350 volts peak-to-peak. The motor controller is capable of independently controlling the motion of each of the scanner motors. The computer contains a function generator card that produces a sinusoidal pulse and an 8-bit A/D board that digitizes the received signals.

The scanner consists of a scan frame, a scan bridge, and a scan head. An image of the scanner is shown in Fig. 9. The scan frame dimensions are 50.8-cm wide by 61.0-cm long by 10.2-cm tall. These dimensions were chosen to enable the scanner to fit inside the environmental chambers where durability testing was being performed. The scan frame incorporates guide rods, a motor, and drive screw to control the motion along the y-axis. The scan bridge uses guides, a motor, and drive screw to govern the motion along the x-axis. The scan head is comprised of the ultrasonic transducers as well as a z-axis motor and a delta-x motor. The z-axis motor is used to raise and lower the transducers. Coupling between the article under test and the transducers is achieved through a thin rubber face plate which is attached to the bottom of the transducers. Bicycle tire patch material proved to be a convenient source for the rubber face plate and provided a good coupling between the test specimen and the transducers. The delta-x motor regulates the spacing between the stationary sending transducer and the movable receiving transducer.
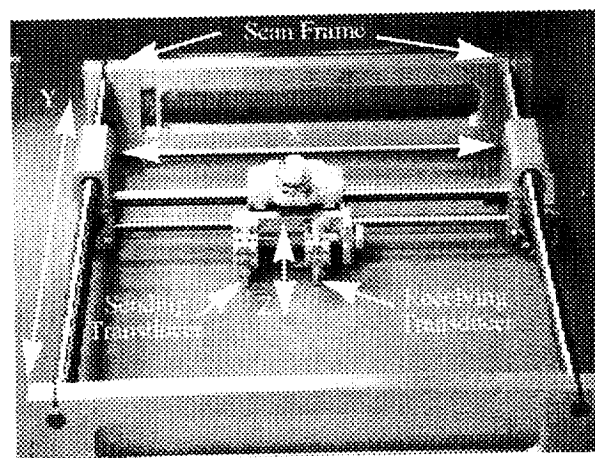

Figure 9. Image of the scanner showing the frame, bridge, and head.

For a scan, the two transducers are used in a pulse/receive arrangement to determine the velocity of the flexural plate mode over a wide frequency range. The

6

receiving sensor is moved in small increments by the delta-x motor in order to assure that the same peak in the waveform is followed over the total separation distance. A schematic of the measurement locations is displayed in Fig. 10. Fig. 11 shows sample signals corresponding to the different receiving transducer positions for a 100 kHz, 4-cycle Gaussian-enveloped sine wave input signal. The signal was received at five different locations separated by 0.5-cm increments. The dashed line on the signals indicates the peak which is followed for the time-of-flight measurements.
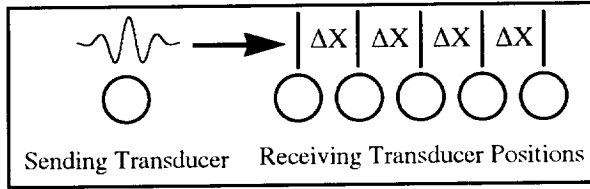

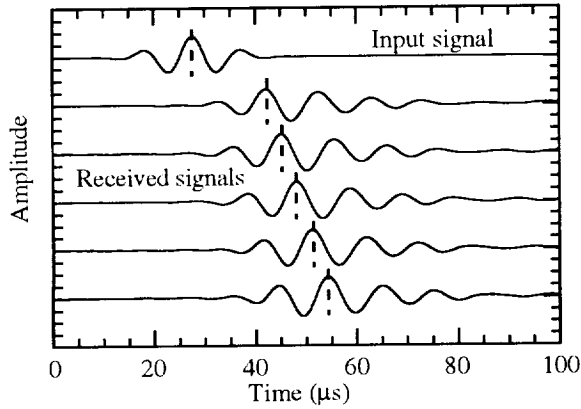Figure 10. Schematic showing the transducer positions for a stiffness measurement.

Figure 11. Sample input and received signals for a 100 kHz input. The separation increment for the received signals was 0.5 cm.

Once the time of arrival from each peak is measured, the velocity at each frequency is calculated from the known transducer separation and the measured time-of-flight. After the velocity as a function of frequency is measured, the bending and out-of-plane shear stiffnesses are obtained from a reconstruction of the flexural mode dispersion curve. The velocity measurements have been shown by Huang, et al.[14] to be accurate and repeatable to within 1% resulting in reconstructed stiffness values repeatable to within 4%.

The x and y-axis motors are used to move the scan head over the surface to map the time-of-flight, velocity, and stiffness of the entire specimen. Access to only one side of the material is required and no couplants are required because the sensors are dry coupled to the surface of the plate

Scanner Accuracy Evaluation

To evaluate the accuracy of the stiffness measurements obtained from Lamb wave velocity measurements, the elastic stiffness was measured in 25 different regions on a large rolled aluminum plate. The plate had dimensions of 50.8 cm by 38.1 cm and a thickness of 0.32 cm. The scan area was 12.0 cm by 12.0 cm with a step size of 3.0 cm and the starting point was 15.0 cm away from the two closest edges of the plate. For the velocity measurement at each location, the sensor separation was varied from 2.75 cm to 4.75 cm in increments of 0.5 cm. An 8-cycle Gaussian-enveloped sine wave was used to generate the signal and the sampling rate was chosen to be 25 MHz. The frequency was swept from 30 to 150 kHz in 10-kHz steps and the velocity at each frequency was measured. Since the material is isotropic, only two independent elastic constants exist. From the data, the dispersion curve was reconstructed and values for the longitudinal and shear modulus which best fit the experimental data were obtained.

For the case of a single isotropic lamina, the stiffness values in Eqs. (4) and (5) take the form[15]

$$A_{44} = A_{55} = 2Gh$$

$$D_{11} = D_{22} = \frac{G^2 h^3}{3(4G - E)}$$

$$D_{16} = 0$$

$$D_{66} = \frac{Gh^3}{6}$$

(10)

where G is the shear modulus, E is the longitudinal modulus, and h is the thickness. Longitudinal and shear modulus values of 67.7 GPa and 25.0 GPa,[16] respectively, were used in the plate theory model to predict a dispersion curve for comparison to the experimental data and the reconstructed dispersion curve.

7

Shown in Fig. 12 is a plot of the average experimental velocity at each frequency, the reconstructed dispersion curve, and the dispersion curve predicted by the plate theory model. As can be seen from the figure, the agreement between the predicted dispersion curve and the reconstructed dispersion curve is excellent. The standard deviations in the velocity at each frequency for the 25 measurement locations were all within 1% of the average with most values being within 0.5% from the average. This small deviation produces error bars on the order of the size of the symbols in the figure. The average reconstructed stiffnesses and the standard deviations for the 25 measurement locations were 66.4 ± 2.0 GPa for the longitudinal modulus and 23.3 ± 1.3 GPa for the shear modulus.

mer matrix composites and taken to be a constant value of 1560 kg/m^3.

The elastic bending stiffness and out-of-plane shear stiffness of the material were computed from a reconstruction of the flexural plate mode dispersion curve. Since the only constants significantly affecting the curve are D_{11} and A_{55} (see Fig. 7), the curve fitting to the experimental data will only use these two parameters. The values of D_{16}, D_{66}, and A_{44} will be set at values obtained from Eqs. (2) and (3). For propagation in the 0° direction, the D_{11} and A_{55} stiffnesses in Eq. (4) were estimated by varying their values to produce the best fit to the experimentally obtained values of ω and k. The stiffnesses D_{22} and A_{44} in Eq. (5) were estimated in a similar manner from data obtained from velocity measurements in the 90° direction.

Sample Reconstruction

Shown in Fig. 13 is the average of ten experimental velocity measurements in the 0° direction for a baseline IM7/5260 sample and one with 2,353 loading cycles at low strain levels and high temperature extremes. Also shown are the reconstructed dispersion curves. The velocity error bars are on the order of the size of the symbols and, therefore, have been omitted from the figure. In the figure, the dispersion curve for the cycled sample is clearly shifted from that of the baseline sample. For the curves shown, the estimated value of A_{55} decreased by 34% and the estimated value of D_{11} increased by 2% for the cycled sample as compared to the baseline sample.
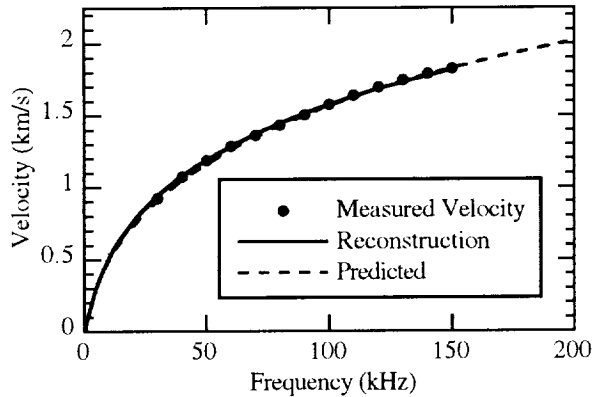

Figure 12. Results for aluminum plate showing the predicted dispersion curve, experimental Lamb wave velocity measurements, and the reconstructed dispersion curve.

Stiffness Measurements in Composites

The Lamb Wave Imager™ was used to measure the stiffness of thermal-mechanically loaded composites at various cycling levels. An 8-cycle Gaussian-enveloped sine wave was used to generate the signal and the received signal was sampled at 25 MHz. The receiving sensor was moved in increments of 0.4 cm for a total distance of 2.0 cm. The frequency was swept in 10-kHz steps from 30 kHz to 200 kHz and the velocity at each frequency was obtained. Due to the large size and the irregular shape of the samples, the density was estimated from common values for poly-

Stiffness Mapping

Stiffness mappings for samples with a variety of loading profiles and times were made in the environmental chambers as well as with the specimens removed from the chambers. With the samples out of the chambers, the entire specimen could be accessed and a stiffness mapping of 75 different regions could be obtained. However, due to the constraints of the chambers, only 20 stiffness measurements in the middle of the specimens could be made for the in situ measurements. Measurements were made both along the length of the samples as well as across the width of the samples to acquire a mapping of A_{55} and D_{11} as well as A_{44} and D_{22}, respectively.
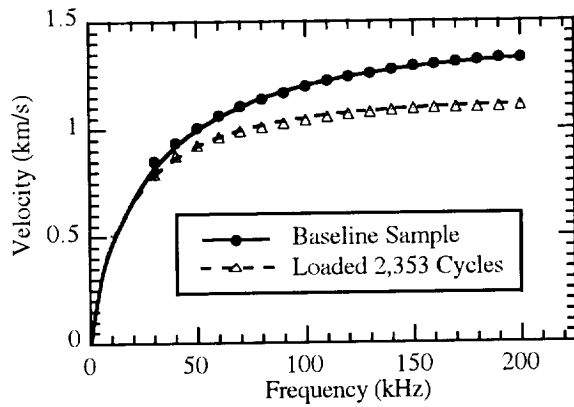
8

Figure 13. Experimental dispersion curves for a baseline IM7/5260 sample and one with 2,353 loading cycles at a low strain/high temperature profile. Also shown are the reconstructed dispersion curves for the baseline (solid line) and cycled (dashed line) samples.

Results

Mapping Results

Sample results of stiffness mappings of A_{55} are shown for the IM7/K3B and the IM7/5260 composites in Fig. 14 and Fig. 15, respectively. In these figures,
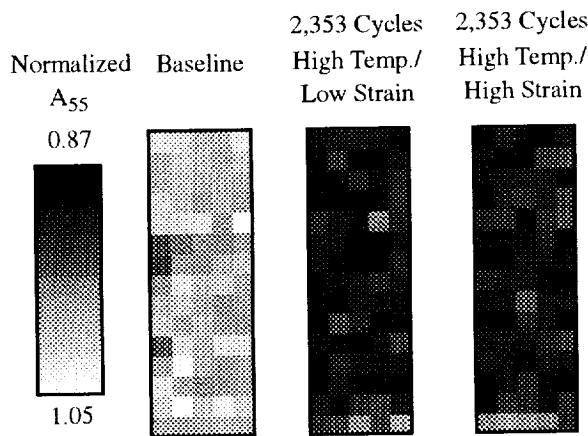

Figure 14. Stiffness mappings of A_{55} for cycled IM7/K3B samples.

the stiffnesses have been normalized to the average stiffness measured for the baseline sample in each set. The higher stiffness values in the regions at the bottom
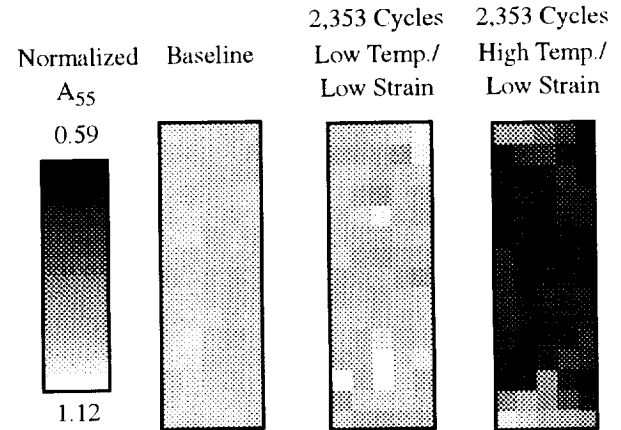
Figure 15. Stiffness mappings of A_{55} for cycled IM7/5260 samples.

of the cycled specimens were due to that portion of the sample being out of the environmental chambers and, therefore, not subjected to the same thermal extremes as the rest of the sample. The average normalized stiffness, A_{55}, and standard deviation for all of the samples measured are compiled in Tables II-V. Also shown in the tables are the normalized values of D_{11} measured for each sample.

Table II. Normalized $0°$ stiffness measurement results for the IM7/K3B low-strain/high-temperature profile samples.

Cycles	Normalized D_{11}	Normalized A_{55}
0	1.00 ± 0.11	1.00 ± 0.02
1,092	1.01 ± 0.22	0.91 ± 0.06
2,339	0.97 ± 0.06	0.90 ± 0.02
2,353	0.90 ± 0.08	0.92 ± 0.02
4,420	0.98 ± 0.11	0.88 ± 0.03

Table III. Normalized $0°$ stiffness measurement results for the IM7/K3B high-strain/high-temperature profile samples.

Cycles	Normalized D_{11}	Normalized A_{55}
0	1.00 ± 0.11	1.00 ± 0.02
1,086	0.96 ± 0.12	0.91 ± 0.04
1,143	0.98 ± 0.09	0.90 ± 0.04
2,353	1.00 ± 0.15	0.91 ± 0.02
4,936	0.93 ± 0.16	0.80 ± 0.05
4,993	0.88 ± 0.08	0.83 ± 0.05

Table IV. Normalized 0° stiffness measurement results for the IM7/5260 low-strain/high-temperature profile samples.

Cycles	Normalized D_{11}	Normalized A_{55}
0	1.00 ± 0.09	1.00 ± 0.01
2,353	1.01 ± 0.14	0.67 ± 0.04
4,706	0.90 ± 0.28	0.36 ± 0.03

Table V. Normalized 0° stiffness measurement results for the IM7/5260 low-strain/low-temperature profile samples.

Cycles	Normalized D_{11}	Normalized A_{55}
0	1.00 ± 0.09	1.00 ± 0.01
1,809	0.92 ± 0.17	0.97 ± 0.09
2,353	0.85 ± 0.11	0.99 ± 0.04
5,637	0.93 ± 0.18	0.96 ± 0.08

Table VI. Normalized 0° stiffness measurement results for the IM7/5260 high-strain/low-temperature profile samples.

Cycles	Normalized D_{11}	Normalized A_{55}
0	1.00 ± 0.08	1.00 ± 0.01
1,759	1.01 ± 0.10	1.01 ± 0.03
2,353	0.96 ± 0.23	0.99 ± 0.07
6,001	1.03 ± 0.24	0.94 ± 0.08

Stiffness results were also obtained for values of A_{44} from measurements in the 90° direction. Sample results of the A_{44} scans for the same samples shown in Figs. 14 and 15 are shown in Figs. 16 and 17, respectively. As with the A_{55} measurements, the stiffnesses have been normalized to the average stiffness obtained for the baseline specimen in each sample set. The average normalized stiffnesses A_{44} and D_{22} as well as standard deviations for the samples are shown in Tables VII-XI.

Table VII. Normalized 90° stiffness measurement results for the IM7/K3B low-strain/high-temperature profile samples.

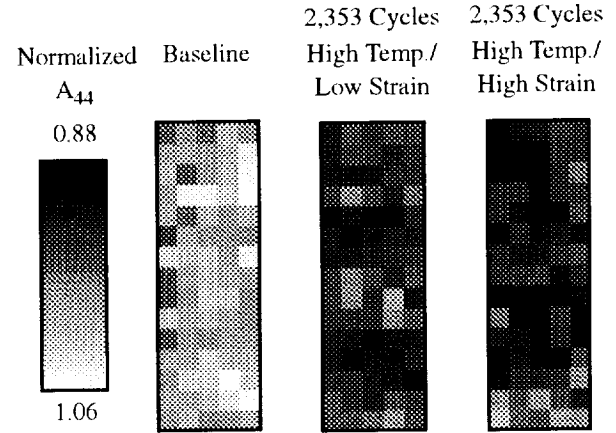| Cycles	Normalized D_{22}	Normalized A_{44}
0	1.00 ± 0.10	1.00 ± 0.02
1,092	0.97 ± 0.14	0.92 ± 0.08
2,339	1.02 ± 0.08	0.95 ± 0.03
2,353	0.86 ± 0.07	0.94 ± 0.02
4,420	0.94 ± 0.11	0.90 ± 0.04

Figure 16. Stiffness mappings of A_{44} for cycled IM7/K3B samples.
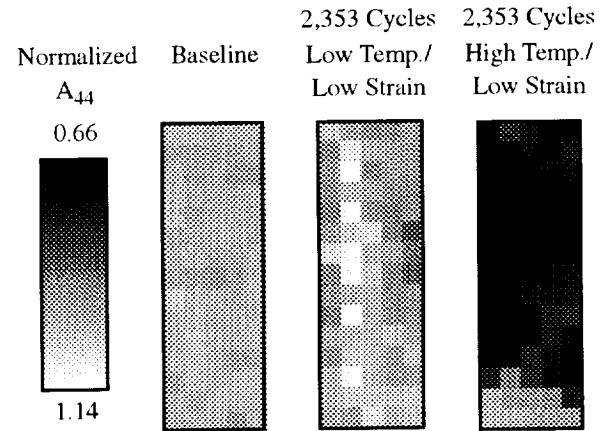
Figure 17. Stiffness mappings of A_{44} for cycled IM7/5260 samples.

Table VIII. Normalized 90° stiffness measurement results for the IM7/K3B high-strain/high-temperature profile samples.

Cycles	Normalized D_{22}	Normalized A_{44}
0	1.00 ± 0.10	1.00 ± 0.02
1,086	0.81 ± 0.06	0.87 ± 0.04
1,143	0.92 ± 0.15	0.88 ± 0.05
2,353	0.94 ± 0.11	0.92 ± 0.02
4,936	0.81 ± 0.06	0.85 ± 0.03
4,993	0.91 ± 0.11	0.87 ± 0.06

Table IX. Normalized 90° stiffness measurement results for the IM7/5260 low-strain/high-temperature profile samples.

Cycles	Normalized D_{22}	Normalized A_{44}
0	1.00 ± 0.06	1.00 ± 0.02
2,353	0.86 ± 0.09	0.73 ± 0.05
4,706	0.77 ± 0.16	0.43 ± 0.03

Table X. Normalized 90° stiffness measurement results for the IM7/5260 low-strain/low-temperature profile samples.

Cycles	Normalized D_{22}	Normalized A_{44}
0	1.00 ± 0.06	1.00 ± 0.02
1,809	0.98 ± 0.22	1.01 ± 0.10
2,353	1.01 ± 0.21	0.99 ± 0.06
5,637	0.83 ± 0.15	0.96 ± 0.08

Table XI. Normalized 90° stiffness measurement results for the IM7/5260 high-strain/low-temperature profile samples.

Cycles	Normalized D_{22}	Normalized A_{44}
0	1.00 ± 0.06	1.00 ± 0.01
1,759	1.03 ± 0.32	1.01 ± 0.12
2,353	1.04 ± 0.29	1.00 ± 0.08
6,001	0.90 ± 0.18	0.90 ± 0.08

IM7/K3B Samples

Shown in Fig. 18 are the normalized values of A_{55} as a function of loading cycles for the IM7/K3B samples which were loaded at high temperatures for both low and high strain levels. The results of A_{44} for the same specimens showed a similar trend. A significant decrease was observed in the out-of-plane stiffness with extended cycling. Additionally, it was observed that the stiffness for the high-strain profile showed a greater decrease than the stiffness for the low-strain profile at levels approaching 5,000 cycles. At this level, the stiffness for the high-strain samples decreased by 20% and the stiffness for the low-strain samples decreased by over 10%.

Plotted in Fig. 19 as a function of loading cycles are the normalized stiffnesses A_{44} and A_{55} for the IM7/K3B specimens loaded at high temperatures and low strain levels. The stiffnesses for the high-strain profiles showed a similar trend. In the figure, the values of A_{55} showed a greater decrease than the values of A_{44}.
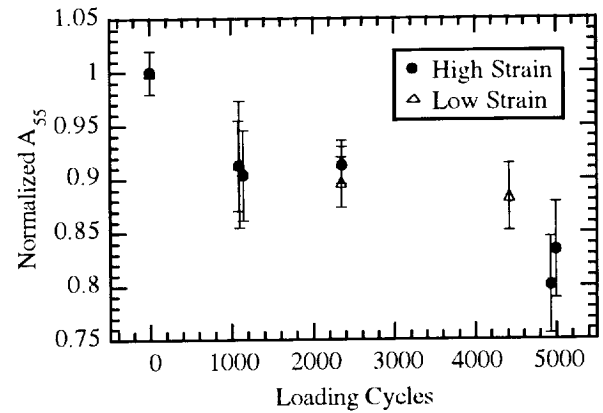

Figure 18. Normalized A_{55} versus loading cycles for IM7/K3B samples loaded at high temperatures for low and high strain levels.
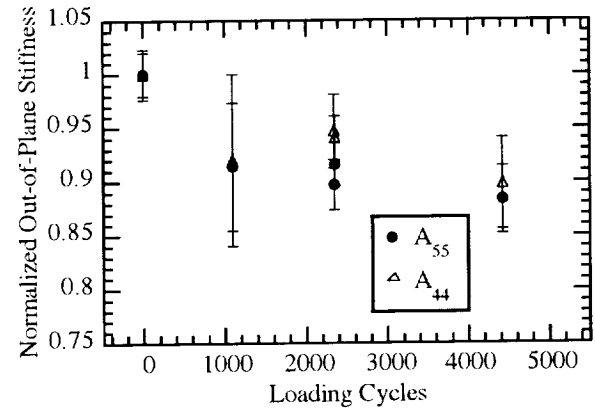

Figure 19. Normalized A_{44} and A_{55} versus loading cycles for IM7/K3B samples cycled at high temperatures and low strain levels.

IM7/5260 Samples

As the tabulated results indicate, there was only about a 5% decrease in the average out-of-plane stiffnesses, A_{44} and A_{55}, for the IM7/5260 samples cycled at low temperature levels. In contrast to the IM7/K3B samples, no discernible difference between high and low strain levels was observed in the out-of-plane stiffness values. Also, there were no appreciable differences between the values of A_{44} and A_{55}. One thing of interest to note, however, are the much larger standard deviations in the cycled samples as compared to the baseline samples.

11

For two IM7/5260 samples, a temperature in excess of the recommended maximum operating temperature (135 °C) was used to accelerate the thermal-mechanical cycling process. The results for the normalized values of A_{55} for specimens loaded at low strain levels for high and low temperature profiles are shown in Fig. 20. The results of the stiffness A_{44} were similar. In Fig. 20, linear fits to the respective data were made in order to display the difference in trends between the samples. The difference in stiffness loss for the samples loaded at high temperatures as compared to the ones loaded at low temperatures was dramatic. Thus, the IM7/5260 specimens did not perform well when subjected to excessive temperatures.
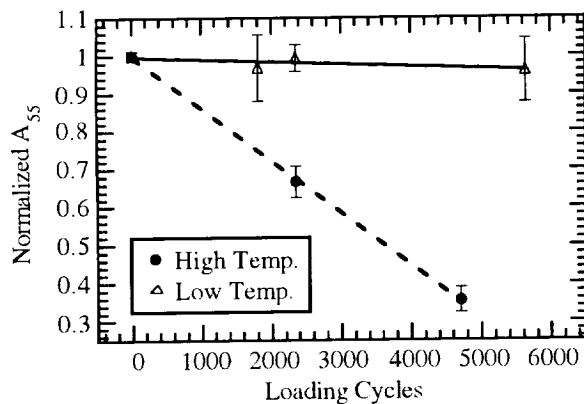

Figure 21. Normalized A_{55} versus loading cycles for IM7/5260 and IM7/K3B samples loaded at low strain levels and high temperature profiles. The solid and dashed lines represent smooth fits to the respective data.

Discussion

In general, the out-of-plane shear carrying capabilities of the composite are matrix dominated, which can be seen from the definition of A_{44} and A_{55} in Eq. (3). It is expected, and previous measurements show,[3,17] that matrix cracking due to mechanical fatigue damage in composites leads to a decrease in elastic moduli. Shown in Fig. 22 is a photomicrograph of the free edge of an IM7/5260 sample which was subjected to high mechanical strains and low temperature levels. The figure clearly shows extensive matrix cracking occurring in the ±45 and 90 degree plies. Photomicrographs taken of the thermal-mechanically loaded IM7/K3B samples also exhibited matrix cracks.

Figure 20. Normalized A_{55} versus loading cycles for IM7/5260 samples cycled at low strain levels for high and low temperature profiles. The solid and dashed lines represent linear fits to the respective data.

Comparison of IM7/K3B and IM7/5250 Samples

A final comparison is made between IM7/5260 and IM7/K3B specimens loaded at identical strain and temperature profiles. Shown in Fig. 21 are the normalized values of A_{55} for samples loaded at low strain levels and a high temperature profile. The results for A_{44} were similar. As can be seen from the figure, the IM7/K3B samples performed much better under higher temperature conditions than the IM7/5260 samples. This is consistent with the fact that the maximum recommended operating temperature of IM7/K3B (177 °C) is greater than the maximum recommended operating temperature of IM7/5260 (135 °C).
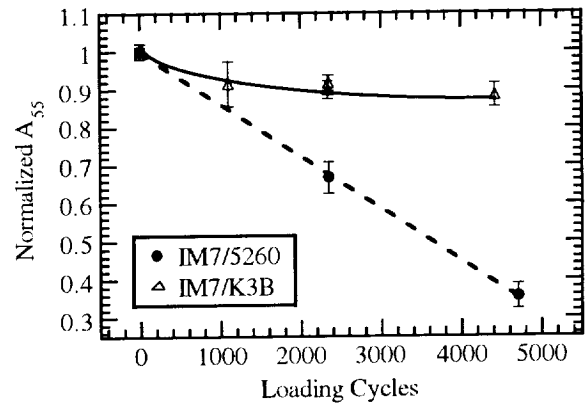
IM7/K3B Samples

Due to matrix cracking, the decrease in the out-of-plane stiffness for the IM7/K3B materials demonstrated in Figs. 14, 16, 18, and 19 was as expected. In addition, if the amount of matrix cracking is related to the strain levels, lower values of A_{44} and A_{55} should be observed in the low-strain samples when compared to the high-strain samples. This was the approximate relationship seen in Fig. 18. Ultrasonic attenuation measurements in these samples have produced similar results suggesting matrix cracking was more prevalent in the high-strain versus low-strain samples.[19]
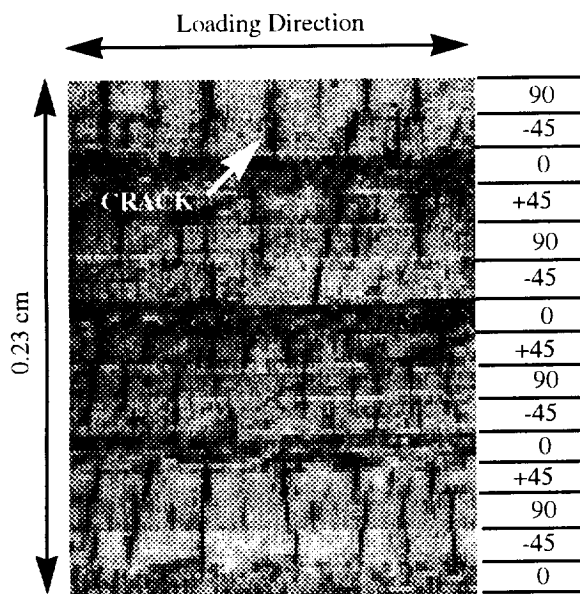
12

Figure 22. Photomicrograph of an IM7/5260 sample showing matrix cracking. Image courtesy of Reference 18.

For the IM7/K3B results shown in Fig. 19, the values of A_{44} did not show as large of a decrease in stiffness with loading cycles as the values of A_{55}. Loading in the 0° direction would tend to produce matrix cracks in the 90° plies as well as the ±45° plies, but not in the 0° plies. Considering that the Lamb wave interaction with cracking is stronger for propagation perpendicular to the crack direction, it is expected that A_{55} will be sensitive to matrix cracking in the 90° and ±45° plies and that A_{44} will be sensitive to cracks in the 0° and ±45° plies. Since 0° ply cracks are not expected to an extensive degree in this loading configuration, only the ±45° ply cracks would adversely affect the value of A_{44}. Therefore, this should lead to a less significant decrease in stiffness for A_{44} than A_{55}, which is consistent with observation in the IM7/K3B samples.

The tabulated values for the IM7/K3B samples indicate an increase in standard deviation for A_{44} and A_{55} in the cycled samples as compared to the baseline samples. The larger standard deviation in the cycled samples was most likely due to localized damaged regions in the specimens due to the loading process. Reports on ultrasonic attenuation measurements in these samples indicated that initially, the damage was localized and, as the number of loading cycles

increased, the damage became more homogeneous throughout the sample.[19]

IM7/5260 Samples

As was seen in Tables IV-VI as well as Tables IX-XI, the standard deviations of the measurements increased substantially during the early stages of cycling for the IM7/5260 samples. The measured values of A_{55} and A_{44} were higher at some locations and lower at others. The higher stiffness values observed might be attributable to additional curing that could occur during the thermal cycling.[20] Additional curing would tend to increase the stiffness of the matrix and thus, increase the out-of-plane stiffness. Countering this effect would be the development of matrix cracks which would tend to lower the stiffness. The juxtaposition of the two processes would lead to little loss in the mean out-of-plane stiffness values at the earlier numbers of cycles, yet would lead to an increase in the variability of the values. Once the curing has reached its maximum possible state and the matrix crack density increases, the matrix damage would dominate and the IM7/5260 specimens should show a general loss in out-of-plane stiffness.

Bending Stiffness

In the tables, the values of D_{11} and D_{22} for both the IM7/K3B and the IM7/5260 samples were reported. Physically, the bending stiffness is controlled by the fibers if the plate bending occurs in the fiber direction and by the matrix if the bending direction of the plate is perpendicular to the fibers. Due to the fact that a quasi-isotropic architecture was used for these samples, the bending stiffness will be affected by both the fiber and the matrix. Since fiber damage was probably not occurring in these samples, the values of D_{11} and D_{22} would predominately reflect the intact fiber load carrying capability and would only be influenced by matrix cracking to a minor degree. Therefore, in general, a very small decrease in the bending stiffness values due to the matrix cracking might be expected.

What is most notable in the tabulated values of D_{11} and D_{22} are that the standard deviations in the bending stiffnesses were 2 to 9 times greater than the standard deviations in the out-of-plane shear stiffnesses. The large standard deviations in the measure-

13

ments represent the insensitivity of the dispersion curve to changes in bending stiffness over the measurement frequency range (30 kHz to 200 kHz). In this region, the parameter dominating the behavior of the curve will be the out-of-plane stiffness (see Fig. 7). Only a few data points exist at the very low frequencies (below 50 kHz) where the bending stiffness controls the behavior of the curve. Due to this lack of data, the constants D_{11} and D_{22} will not be as accurate as the constants A_{55} and A_{44}. Although the tables show a small increase in some of the values of D_{11} and D_{22} instead of the expected small decrease, the large standard deviations associated with the measurement cover up any true significance.

Conclusions

Lamb wave imaging is a method for nondestructively measuring the elastic properties of a material. The scanner requires access to only one side of a specimen with no immersion or couplants. It has been shown by this study to be an effective method in providing a quantitative measure of stiffness changes due to thermal-mechanical loading in composite materials. The IM7/K3B samples which were loaded at high temperatures and high strain levels showed a 20% decrease in stiffness after 4,936 cycles. The IM7/5260 samples loaded at low temperatures for both high and low strain levels showed less than a 10% decrease in stiffness after 6,001 cycles. However, the IM7/5260 samples which were subjected to excessively high temperatures and low strain levels showed a decrease in stiffness of over 60% after 4,706 cycles. The bending stiffnesses showed few effects of thermal-mechanical loading due to their insensitivity to matrix cracking as well as the large standard deviations arising from the frequency range used for the measurements. All of the samples showed an increase in stiffness variation for the thermal-mechanically cycled specimens.

References

1. M.R. Karim, A.K. Mal, and Y. Bar-Cohen, "Inversion of Leaky Lamb Wave Data by Simplex Algorithm," J. Acoust. Soc. Am. **88**, 482-491 (1990).

2. Ajit K. Mal, Shyh-Shiuh Lih, and Yoseph Bar-Cohen, "Ultrasonic Determination of the Elastic Properties of Unidirectional Composites," in *Review of Progress in Quantitative Nondestructive Evaluation*, Vol. 12, edited by D.O. Thompson and D.E. Chimenti (Plenum Press, New York, 1993), pp. 1233-1240.

3. Michael D. Seale, Barry T. Smith, and W.H. Prosser, "Lamb Wave Assessment of Fatigue and Thermal Damage in Composites," J. Acoust. Soc. Am. **103** (5), Pt. 1, 2416-2424 (1998).

4. V. Dayal and V.K. Kinra, "Ultrasonic NDE of Composites for Transverse Cracking," in *Optical Methods in Composites: Proceedings of the SEM Fall Conference on Experimental Mechanics*, (A88-13876 03-24), (Society for Experimental Mechanics, Inc., Bethel, CT, 1986), pp. 17-22.

5. B. Tang and E.G. Henneke, II, "Lamb-Wave Monitoring of Axial Stiffness Reduction of Laminated Composite Plates," Mater. Eval. **47**, 928-934 (1989).

6. V. Dayal, V. Iyer, and V.K. Kinra, "Ultrasonic Evaluation of Microcracks in Composites," in *Advances in Fracture Research: Proceedings of the Seventh International Conference on Fracture* (ICF7), Vol. 5, (A90-41276 18-39), (Pergamon Press, New York, 1989), pp. 3291-3300.

7. J.-H. Shih, A.K. Mal, and M. Vemuri, "Plate Wave Characterization of Stiffness Degradation in Composites During Fatigue," Res. Nondestr. Eval. **10**, 147-162 (1998).

8. Yoseph Bar-Cohen, Shyh-Shiuh Lih, Ajit Mal, and Zensheu Chang, "Rapid Characterization of the Degradation of Composites Using Plate Wave Dispersion Data," in *Review of Progress in Quantitative Nondestructive Evaluation*, Vol. 17, edited by D.O. Thompson and D.E. Chimenti (Plenum Press, New York, 1998), pp. 1171-1176.

9. Bhagwan D. Agarwal and Lawrence J. Broutman, *Analysis and Performance of Fiber Composites*, 2nd Edition (John Wiley & Sons, Inc., New York, NY, 1990), p. 153.

10. B. Tang, E.G. Henneke II, and R.C. Stiffler, "Low Frequency Flexural Wave Propagation in Laminated Composite Plates," in *Acousto-Ultrasonics Theory and Application*, edited by John C. Duke, Jr. (Plenum Press, New York and London, 1987), pp. 45-65.

11. S.B. Dong and K.H. Huang, "Edge Vibrations in Laminated Composite Plates," J. Appl. Mech. **52**, 433-438 (1985).

12. Subhendu K. Datta, A.H. Shah, and W. Karunasena, "Wave Propagation in Composite Media and Material Characterization," in *Elastic Waves and Ultrasonic Nondestructive Evaluation*, edited by S.K. Datta, J.D. Achenbach, and Y.S. Rajapakse (Elsevier Science Publishers B.V., North-Holland, 1990), pp. 159-167.

13. William H. Prosser, "The Propagation Characteristics of the Plate Modes of Acoustic Emission Waves in Thin Aluminum Plates and Thin Graphite/Epoxy Composite Plates and Tubes," *NASA Technical Memorandum 104187*, November 1991.

14. W. Huang, S.M. Ziola, J.F. Dorighi, and M.R. Gorman, "Stiffness Measurement and Defect Detection in Laminated Composites by Dry-Coupled Plate Waves," in *Process Control and Sensors for Manufacturing*, edited by R.H. Bossi and D.M. Pepper (SPIE, Bellingham, Washington, 1998), pp. 66-76.

15. R.M. Christensen, *Mechanics of Composite Materials* (John Wiley & Sons, New York, New York, 1979), p. 165.

16. B.A. Auld, *Acoustic Fields and Waves in Solids* (Robert E. Krieger Publishing Company, Malabar, Florida, 1990), Vol. 1, p. 379.

17. Timothy W. Coats and Charles E. Harris, "Experimental Verification of a Progressive Damage Model for IM7/5260 Laminates Subjected to Tension-Tension Fatigue," J. Compos. Mater. **29** (3), 280-305 (1995).

18. Private communication, Karen Whitley of NASA Langley Research Center and Steven Grossen Lockheed Martin.

19. Eric I. Madaras, William P. Winfree, and Patrick H. Johnston, "Ultrasonic Studies of Composites Undergoing Thermal and Fatigue Loading," in *Review of Progress in Quantitative Nondestructive Evaluation*, edited by D.O. Thompson and D.E. Chimenti (Plenum Press, New York, 1998), Vol. 17, pp. 1237-1244.

20. W.M. Johnston and T.S. Gates, "The Effects of Stress and Temperature on the Open-Hole Tension Fatigue Behavior of a Graphite/Bismaleimide Composite," in *Composite Materials: Fatigue and Fracture, Seventh Volume, ASTM STP 1330*, edited by R.B. Bucinell (American Society for Testing and Materials, West Conshohocken, PA, 1998), pp. 179-198.

15

REPORT DOCUMENTATION PAGE

Public reporting burden for this collection of information is estimated to average 1 hour per response, including the time for reviewing instructions, searching existing data sources, gathering and maintaining the data needed, and completing and reviewing the collection of information. Send comments regarding this burden estimate or any other aspect of this collection of information, including suggestions for reducing this burden, to Washington Headquarters Services, Directorate for Information Operations and Reports, 1215 Jefferson Davis Highway, Suite 1204, Arlington, VA 22202-4302, and to the Office of Management and Budget, Paperwork Reduction Project (0704-0188), Washington, DC 20503.

1. AGENCY USE ONLY *(Leave blank)*	2. REPORT DATE December 2000	3. REPORT TYPE AND DATES COVERED Technical Memorandum

4. TITLE AND SUBTITLE
Use of Guided Acoustic Waves to Assess the Effects of Thermal-Mechanical Cycling on Composite Stiffness

5. FUNDING NUMBERS
WU 537-06-33-20

6. AUTHOR(S)
Michael D. Seale and Eric I. Madaras

7. PERFORMING ORGANIZATION NAME(S) AND ADDRESS(ES)
NASA Langley Research Center
Hampton, VA 23681-2199

8. PERFORMING ORGANIZATION REPORT NUMBER
L-18046

9. SPONSORING/MONITORING AGENCY NAME(S) AND ADDRESS(ES)
National Aeronautics and Space Administration
Washington, DC 20546-0001

10. SPONSORING/MONITORING AGENCY REPORT NUMBER
NASA/TM-2000-210628

11. SUPPLEMENTARY NOTES
Michael D. Seale: National Research Council Research Associate at NASA Langley Research Center, Hampton, VA; Eric I. Madaras: NASA Langley Research Center, Hampton, VA.

12a. DISTRIBUTION/AVAILABILITY STATEMENT
Unclassified–Unlimited
Subject Category 24   Distribution: Nonstandard
Availability: NASA CASI (301) 621-0390

12b. DISTRIBUTION CODE

13. ABSTRACT *(Maximum 200 words)*
The introduction of new, advanced composite materials into aviation systems requires a thorough understanding of the long-term effects of combined thermal and mechanical loading. As part of a study to evaluate the effects of thermal-mechanical cycling, a guided acoustic (Lamb) wave measurement system was used to measure the bending and out-of-plane stiffness coefficients of composite laminates undergoing thermal-mechanical loading. The system uses a pulse/receive technique that excites an antisymmetric Lamb mode and measures the time-of-flight over a wide frequency range. Given the material density and plate thickness, the bending and out-of-plane shear stiffnesses are calculated from a reconstruction of the velocity dispersion curve. A series of 16 and 32-ply composite laminates were subjected to a thermal-mechanical loading profile in load frames equipped with special environmental chambers. The composite systems studied were a graphite fiber reinforced amorphous thermoplastic polyimide and a graphite fiber reinforced bismaleimide thermoset. The samples were exposed to both high and low temperature extremes as well as high and low strain profiles. The bending and out-of-plane stiffnesses for composite samples that have undergone over 6,000 cycles of thermal-mechanical loading are reported. The Lamb wave generated elastic stiffness results have shown decreases of up to 20% at 4,936 loading cycles for the graphite/thermoplastic samples and up to 64% at 4,706 loading cycles for the graphite/thermoset samples.

14. SUBJECT TERMS
Lamb wave; Nondestructive evaluation; Thermal-mechanical durability; Ultrasonics

15. NUMBER OF PAGES
20

16. PRICE CODE
A03

17. SECURITY CLASSIFICATION OF REPORT	18. SECURITY CLASSIFICATION OF THIS PAGE	19. SECURITY CLASSIFICATION OF ABSTRACT	20. LIMITATION OF ABSTRACT
Unclassified	Unclassified	Unclassified	UL